Biosensors and Bioelectronics 123 (2019) 260–268

Contents lists available at ScienceDirect

Biosensors and Bioelectronics

journal homepage: www.elsevier.com/locate/bios

Recognition of protein biomarkers using epitope-mediated molecularly imprinted films: Histidine or cysteine modified epitopes?

Raoul Tchinda, Anna Tutsch, Bianca Schmid, Roderich D. Süssmuth, Zeynep Altintas*

Institute of Chemistry, Technical University of Berlin, Straße des 17. Juni 124, 10623 Berlin, Germany

ARTICLE INFO

Keywords:
Cysteine modified epitope imprinting
Histidine modified epitope imprinting
Neuron specific enolase
Cancer biomarker
Electrochemical sensor
Protein recognition

ABSTRACT

This research aims to engineer molecularly imprinted polymer (MIP)-based synthetic receptors for the molecular recognition of neuron specific enolase (NSE) biomarker. The synthetic peptide derived from the NSE was synthesized along with its cysteine and histidine modified versions. The modified peptides were utilized as templates for molecular imprinting, which was achieved by combination of epitope- and electrochemical surface imprinting strategy. The subsequently generated imprinted cavities were used for the detection of the NSE derived peptide and NSE. The imprints created with cysteine (CME) and histidine modified epitopes (HME) could detect the peptide in a concentration range of 2–128 μM and 15.6 nM to 128 μM, respectively. The recognition of NSE was achieved by the same imprints in a linear range of 1–64 ng mL^{-1} (CME) and 0.25–64 ng mL^{-1} (HME), respectively. The target molecules bound to the control polymer very weakly, confirming the high selectivity of the MIP cavities. Selectivity studies resulted in imprinting factors of 8.8 and 11 for the CME and HME imprints, respectively. The affinity analyses provided dissociation constants of 2.3×10^{-10} M and 3×10^{-11} M for NSE recognition using the corresponding epitope imprints. Cross-reactivity studies with non-specific molecules proved high specificity of the artificial receptors for the targets.

1. Introduction

Cancer is among the major causes of death worldwide, particularly with higher mortality rates of some types such as lung and liver cancers (American Cancer Society, 2017). The cheap, efficient, fast, and easy-to-use diagnostic tools can enormously reduce the mortality rates by providing early detection (Altintas, 2017). Neuron specific enolase (NSE) is a reliable tumour biomarker whose presence in body fluids is an indicator of small cell lung cancer (SCLC) (Altintas and Tothill, 2013). It is a cell specific isoenzyme (47 kDa) of the glycolytic enzyme enolase, which is highly specific for neurons and neuroendocrine cells (Marangos, 1987). Measuring the amounts of NSE in blood can help early diagnosis by giving information on the clinical stages of SCLC development (Altintas and Tothill, 2013). The level of NSE in healthy individuals is < 15 ng mL^{-1} and this concentration exceeds 80 ng mL^{-1} in extensive SCLC patients (Cooper, 1994; Cooper et al., 1985). Currently, the detection of NSE mainly relies on immunoassays using different labels through fluoroimmunoassay (Cao et al., 2011), radioimmunoassay (RIA) (Huang et al., 2017), enzyme-linked immunosorbent assay (ELISA) (Vermuyten et al., 1990; Shibayama et al., 2001) or electro/chemiluminescence assay (Schmidt et al., 2014; Fu et al., 2012). These detection methods are well known for their efficacy and specificity toward biomarkers but are prone to the use of bioreceptors such as antibodies and enzymes whose fragility and cost make them expensive. In order to tackle these drawbacks, synthetic receptors have been developed to attain the similar specificity, recognition ability, and selectivity (Zhang et al., 2018; Cecchini et al., 2017).

Molecular imprinting provides artificial, tailor-made receptors that are able to specifically recognize target molecules, thus mimicking natural bioreceptors (Wulff and Sarhan, 1972). A molecularly imprinted polymer (MIP) is usually synthesized through a combination of a variety of components forming an imprint complementary to a specific target. These components include a functional monomer, a cross-linker, an initiator, and a solvent depending on the imprinting strategy being employed (Altintas et al., 2015a, 2015b). Many imprinting strategies have been reported in literature that are highly successful for small molecules such as drugs (Li et al., 2012; Pernites et al., 2011; Altintas et al., 2015c), toxins (Abdin et al., 2015) and peptides (Chen et al., 2016). On the other hand, protein imprinting is still a challenge due to the complex nature of proteins partly influenced by their aqueous environment that may lead to conformational changes during polymerization and less efficient cavities (Erdossy et al., 2016; Kryscio et al., 2012). Another limitation is the large size of proteins which makes their removal difficult from the polymer network. It is worth

* Corresponding author.
E-mail address: zeynep.altintas@tu-berlin.de (Z. Altintas).

https://doi.org/10.1016/j.bios.2018.09.010
Received 30 June 2018; Received in revised form 28 August 2018; Accepted 1 September 2018
Available online 07 September 2018
0956-5663/

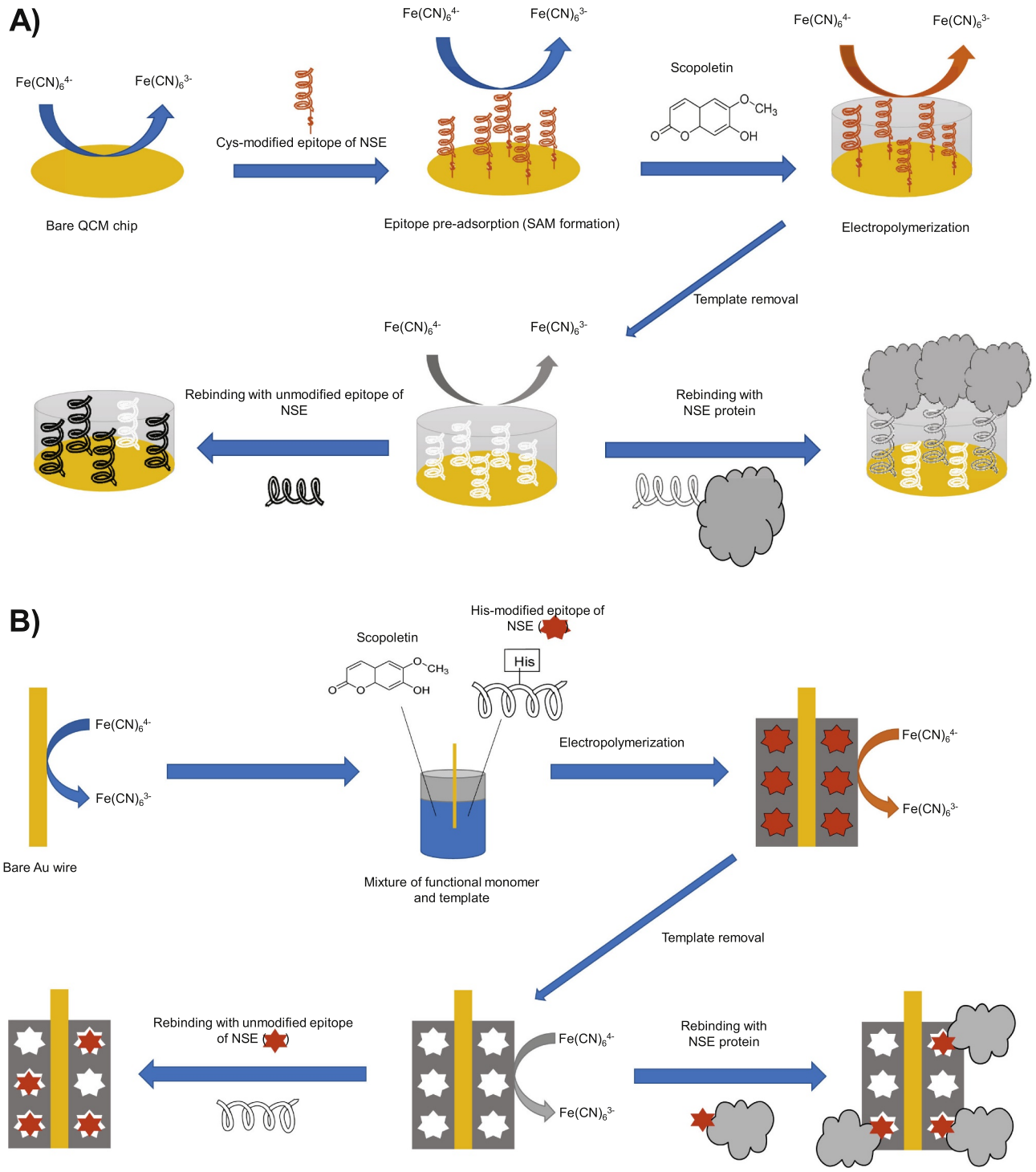

Scheme 1. The principle of protein biomarker recognition using the epitope-mediated electrosynthesized MIPs based on cysteine **(A)** and histidine **(B)** modified epitope imprinting. Every step of the assay was characterized by the redox couple ferri/ferrocyanide.

noting that the whole protein imprinting is also quite expensive as it requires using high concentrations of proteins during the synthesis (Zhang et al., 2018). These challenges can be avoided by implementing epitope imprinting in which a small fragment of the protein is imprinted, whose corresponding cavities are capable of recognizing the whole protein. The sequence to be imprinted usually consists of several amino acids and could be modified depending on the investigation purpose (Feng et al., 2014; Karimian et al., 2014; Lautner et al., 2011; Moreira et al., 2014; Nishino et al., 2006; Viswanathan et al., 2012). Hoshino et al. (2010) reported the recognition, neutralization, and clearance of the melittin toxin (a peptide consisting of 26 amino acids) from the bloodstream of living mice. Imprinting of proteins, such as cytochrome c (Dechtrirat et al., 2012), ferritin (Bosserdt et al., 2015), human serum albumin (Cieplak et al., 2015; Stojanovic et al., 2017) and bovine serum albumin (Chen et al., 2012), has also been reported by many research groups with a few reporting on MIP-based electrochemical sensors for cancer biomarker detection.

In this work, we report on cysteine and histidine modified epitope imprinting for electrochemical sensing of NSE for the first time (Scheme 1). The electrochemically formed MIPs on gold electrodes could

recognize and capture the NSE derived synthetic peptide and NSE by using a redox probe whose oxidation provided information for the binding of target molecules to the synthesized cavities. The electropolymerization method offers many advantages over other polymerization techniques: 1) Easy control of the polymerization thickness, hence, template entrapment due to thick and dense polymer films is minimized and better template removal can be achieved. 2) The polymer film is formed directly from the aqueous solution which is favourable for the imprinting of biological molecules such as peptides and proteins. The majority of the other MIP manufacturing methods are only successful with organic solvents not suited for work with proteins. Herein, we introduce a novel technique for protein recognition using epitope-mediated electrosynthesized MIPs. For this, we synthesized a surface exposed 12-amino acid sequence of NSE (AMRLGAEVYHTL, residues 180–191) to establish sensor arrays. We also synthesized its cysteine (**C**AMRLGAEVYHTL) and histidine modified versions (AMRLGA**H**EVYHTL) for use in imprinting process. The biosensing method was then transferred for sensitive and specific detection of NSE biomarker. The peptide imprints were formed as a thin film on gold quartz crystals or gold wires. The template removal and target binding were detected by probing the relevant permeability changes of the MIP films to the redox markers using cyclic voltammetry (CV), square wave voltammetry (SWV) and atomic force microscopy (AFM) techniques. The efficiencies of the two imprinting methods were compared in terms of sensitivity, selectivity and specificity.

2. Experimental section

All reagents and chemicals, electrochemical measurements and the related equipment, the cleaning protocols of quartz crystal microbalance (QCM) chips and gold wires, and peptide synthesis are detailed in Supporting information.

We introduced two epitope imprinting approaches in this study: The first approach (Section 2.1) requires using the pre-adsorbed cysteine modified epitope (CME) template on the QCM gold surface followed by electropolymerization around the template and subsequent template removal by applying an anodic potential. The second approach (Section 2.2) involves direct electropolymerization of the template (the histidine modified epitope, HME) together with the scopoletin monomer on a gold wire followed by template removal using alkaline treatment.

2.1. Epitope imprinting using cysteine modified peptide

For the MIP preparation, the CMEs (50 μM) in TCEP buffer (pH 7.3) were first immobilized on the QCM gold chip based on self-assembled monolayer (SAM) formation for a total period of 3 h. Adsorption was facilitated by the thiol side chain of cysteine, which has high affinity toward gold, in the epitope sequence. A 0.5 mM scopoletin prepared in 0.1 M NaCl was deposited onto the QCM gold surface by applying a multistep amperometry technique for electropolymerization. The optimal polymerization cycle was initially determined based on the comparative rebinding efficiencies (Fig. S1). Accordingly, the electrodeposition was executed by 50 pulse pairs starting with 0 V for 5 s and followed by 0.9 V for 1 s. The polymerization mixture was then removed from the electrochemical cell and rinsed with distilled water several times. A thin film was formed with these parameters. The subsequent template removal was enabled by applying anodic desorption with the multiple pulse amperometry technique at 0.9 V for 30 s. The MIP films were thoroughly washed with distilled water to remove any remaining epitope templates from the surface. The non-imprinted polymer (NIP) film was synthesized as control using the same procedure in the absence of the template and the selectivity of the cavities was investigated in comparison with the MIPs. The imprinting factor (IF) was calculated based on these comparative studies by taking the signal ratio between the MIPs and NIPs (Zhang et al., 2018). The MIP cavities were used for the recognition and detection of the NSE derived peptide and the NSE biomarker.

2.2. Epitope imprinting using histidine modified peptide

The MIPs using the HME peptide were synthesized by electropolymerizing the aqueous mixture of the template (50 μM histidine containing peptide) and scopoletin monomer (0.5 mM) on the gold wire surface. The optimum electropolymerization condition was achieved by multistep amperometry technique with 30 pulse pairs (the optimal polymerization cycle, see Fig. S2) starting with 0 V for 5 s and followed by 0.9 V for 1 s. The template removal was performed by applying alkaline treatment in 0.1 M NaOH solution for 40 min followed by thorough washing with distilled water. The prepared MIP sensor was then used for target detection.

The NIP was prepared using the same procedure without the presence of the template and the non-specific interaction of the target molecule with the NIP was investigated to evaluate the imprinting factor.

2.3. Target detection

The imprints were initially used for recognition and detection of the NSE derived synthetic peptide (AMRLGAEVYHTL). The samples were prepared in phosphate buffer (pH 7.3) and the detection of the peptide was investigated in a concentration range of 1–128 μM and 7.5 nM to 128 μM using the cysteine and histidine modified epitope imprinting approaches, respectively. Each sample was injected into the electrochemical cell and incubated for 30 min prior to electrochemical measurements by SWV using the redox marker. On the other hand, the detection of NSE was investigated in a concentration range of 1–64 ng mL^{-1} (CME peptide) and 0.25–64 ng mL^{-1} (HME peptide) using methods 1 and 2. The binding of the protein to the cavities was measured using the SWV technique. The affinities between the imprints and the target molecules were analyzed by determining the dissociation constant K_d via the Scatchard plot. Accordingly, raw SWV data were converted into signal suppression data as percentage. This standardization of values made them comparable between the individual experiment series. The data obtained in terms of signal suppression indicated the relative signal of the sensor for each sample measurement. A plot of relative signal of redox marker (%) vs relative signal of redox marker (%) divided by epitope or protein concentration (μM or ng mL^{-1}) gave a straight line where the slope (m) was used to calculate K_d (in M or ng mL^{-1}) using Eq. (1) (Zhang et al., 2018).

$$m = -\frac{1}{K_d} \quad (1)$$

2.4. AFM characterization of MIP and NIP films

Atomic force microscopy (AFM) was used to characterize the polymer films on the QCM chip surfaces. For AFM-based surface characterization, the MIPs and NIPs were prepared by using the methods described in Sections 2.1 and 2.2. The template removal was also achieved according to the polymerization procedures described in Sections 2.1 and 2.2 for cysteine and histidine modified epitope peptides, respectively. Every step of the imprinting process (bare gold surface, MIP synthesis and template removal) was followed by AFM (NanoWizard II, JPK Instruments AG., Germany). The cross-section analysis, the root mean square (RMS) roughness and the surface topology values of each surface were evaluated. The measurements were performed in dry state using intermittent contact mode. Commercially available AFM probe (TAP300 AL-G) from Budget Sensors (Innovative Solutions Bulgaria Ltd., Bulgaria) was used on cantilevers with a resonance frequency in the range of 300 ± 100 kHz. The scanning line rate was 0.2–0.5 Hz. The samples were measured in different scanning areas (10 μm × 10 μm, 3 μm × 3 μm and 1 μm × 1 μm) to investigate

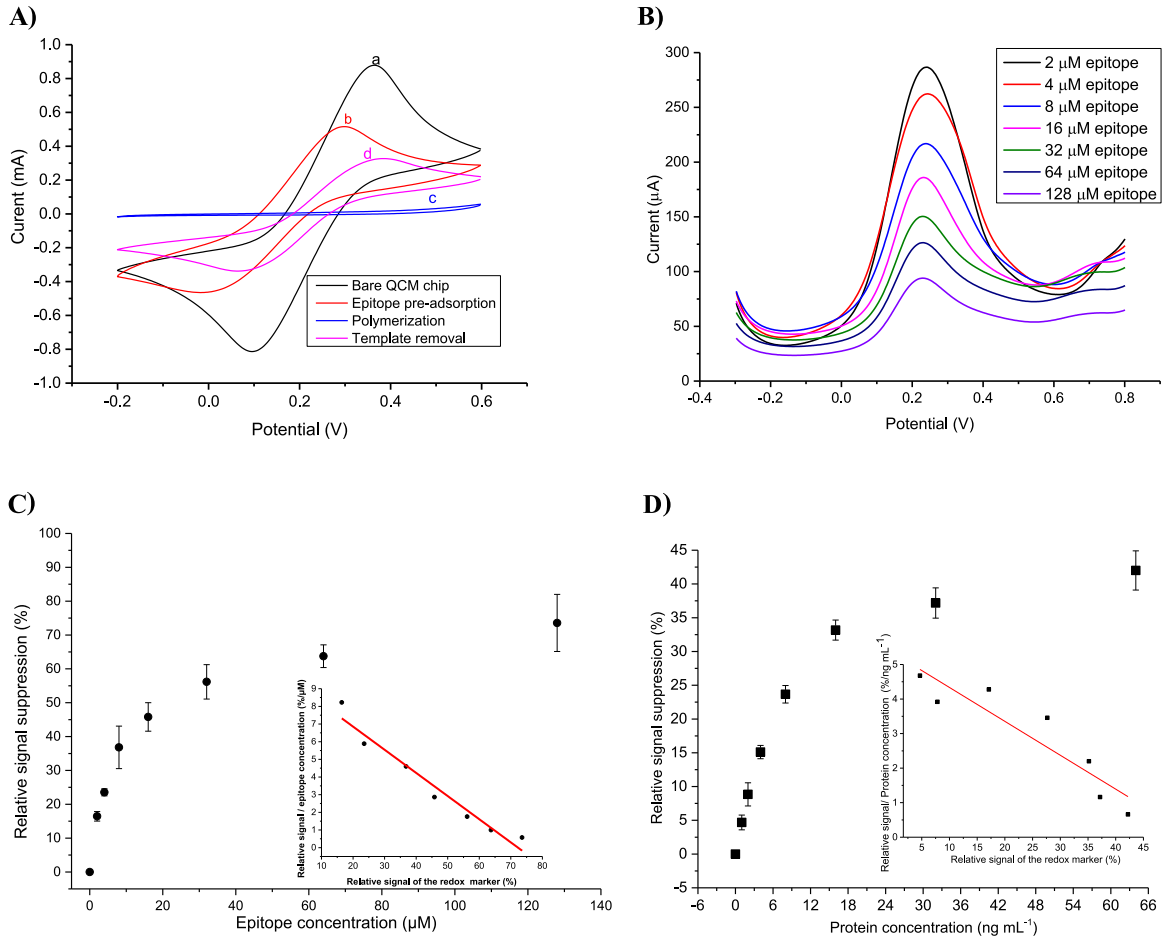

Fig. 1. A) Characterization of each step of the cysteine-modified peptide epitope MIP synthesis using cyclic voltammetry (CV): Voltammograms recorded in $K_3[Fe(CN)_6]$ (5 mM), $K_4[Fe(CN)_6]$ (5 mM)/potassium chloride (0.1 M) for the bare gold electrode (a), SAM formation (b), polymerization of scopoletin (c) and template removal (d). **B)** Square wave voltammetry detection of the NSE derived peptide in the concentration range of 2—128 μM using the cysteine modified epitope imprints. **C)** Concentration-dependent peptide detection using the MIP sensor prepared with cysteine modified peptide epitope imprints. Inset: The Scatchard plot, $K_d = 7.6 \times 10^{-6}$ M. **D)** The detection of NSE biomarker in the linear range of 1—64 ng mL^{-1} using the MIP sensor. Inset: the Scatchard plot, K_d value: 2.3×10^{-10} M.

the surfaces in detail. Phase image analysis was also performed in a 1 μm^2 scanning area to visualize different chemical components on the templated and template free surfaces. The AFM measurements of the polymer films were carried out at room temperature and under dry conditions. The images were processed by using JPKSPM Data Processing software.

2.5. Cross-reactivity test

The specificity and selectivity of the synthesized MIPs were tested by investigating the cross-reaction of the MIPs with non-specific peptides (control peptide 1: LKAVDHINST and control peptide 2: CKGVLKAVDHINSTIAPC) and proteins (bovine serum albumin, BSA) at a fixed concentration of 30 ng mL^{-1}. The target molecules (the NSE derived synthetic peptide and NSE biomarker) were also tested as part of this experiment under the same conditions. All the samples were prepared in phosphate buffer and incubated for 30 min on the CME- and HME-MIP electrodes. Each MIP film was prepared independently for testing each analyte. The relative signal suppression was calculated for the samples and the results were demonstrated in comparison.

3. Results and discussion

3.1. Cysteine-modified epitope imprinting

The MIP was prepared as illustrated in Scheme 1A using scopoletin as a functional monomer. The polyscopoletin MIP films provide non-conductive and hydrophilic polymers, and allow non-covalent interactions with the epitope template (Bosserdt et al., 2015). Every step of the electro-synthesized cysteine-modified peptide epitope MIP was characterized using CV and SWV techniques in the presence of a redox couple. The oxidation and reduction peaks of the CV curves were clearly suppressed after pre-adsorption of the cysteine modified peptide epitope on the gold surface (SAM formation) (Fig. 1A, curves a and b). The signal suppression drastically increased after the formation of polyscopoletin polymer around the template (Fig. 1A, curve c). The removal of the template, as a result of anodic potential application to the surface, relatively increased the oxidation and reduction peaks when compared to the polymerization process (Fig. 1A, curve d). During the template removal step the applied potential oxidized the thiol groups of cysteine peptide attached to the Au, and thus removed the template. Pre-adsorption of the template molecule via the thiol group of cysteine on gold surface is beneficial for the formation of a stable MIP film, as it can avoid non-specific interactions and form stable cavities. The corresponding SWV graphs of the same surfaces showed the peak signals of 963.3 μA, 465.4 μA, 91.4 μM and 343.11 μM for the bare chip, the pre-adsorbed template (SAM formation), the polymerization, and the template removal at around 0.2 V (Fig. S3), which are all in good agreement with CV results.

The thickness of the MIP films plays a key role to obtain successful imprints for target detection (Zhang et al., 2018). Thinner films are preferable over thicker films during MIP synthesis partly due to the

possibility of template entrapment and thus difficult template removal. Herein, 50 polymerization cycles were found optimal as it supplied a sufficient film thickness that allowed removing the template easily. The NIPs prepared under the same conditions without using the template molecule led to different peak heights when compared to the MIPs (Fig. S4, left panel). This is most likely due to the presence of the cysteine modified epitope template in the latter case that led to a relatively thicker polymer on the surface. The current peak heights of 98.02 μA and ~ 64.1 μA obtained for the NIP and the MIP by SWV technique confirmed this hypothesis (Fig. S4, right panel).

3.2. Target detection assays using cysteine-modified epitope imprints

The detection of NSE derived peptide and NSE protein using the cysteine-modified peptide epitope imprints was investigated over a wide concentration range: The imprints recognized the peptide target in the range of 2–128 μM and this could be demonstrated by square wave voltammograms (Fig. 1B). The raw data of seven separate experiments demonstrated a small variation and resulted in a R^2 value of 0.99 when subjected to the logarithmic regression analysis (Fig. S5). The raw data of peptide detection assays were converted into the relative signal suppression (Fig. 1C) and the affinity determination was made based on these data (Fig. 1C, inset: Scatchard plot). The Scatchard plot resulted in a dissociation constant of 7.6×10^{-6} M.

The recognition of whole protein was investigated under the same conditions using the epitope imprinted cavities. NSE could be measured in a linear concentration range from 1 ng mL^{-1} to 64 ng mL^{-1} (Fig. S6, Fig. 1D). The lower concentration of NSE (0.5 ng mL^{-1}) demonstrated a current signal that was similar to that of template removal signal. The limit of detection for protein recognition was therefore 1 ng mL^{-1}. A high affinity between the epitope imprints and the NSE protein was found based on the Scatchard plot, which revealed a K_d of 2.3×10^{-10} M. This affinity is much higher than those of many natural and synthetic receptors reported so far. Moreover, CME imprints provided clearly higher affinity and sensitivity than those of unmodified epitope imprints for both NSE derived peptide (K_d: 15.44×10^{-6} M, LOD: 4 μM) and NSE protein (K_d: 3.4×10^{-10} M, LOD: 2 ng mL^{-1}) (Fig. S7). This is most likely due to more random orientation of unmodified epitopes during the polymerization process (Jetzschmann et al., 2018). A recent work has reported a K_d of 5×10^{-7} M for a polyscopoletin-based MIP using protein imprinting (Zhang et al., 2018). Dechtrirat et al. (2012) used cysteine-modified peptide epitope imprints for the detection of cytochrome c-derived peptide and cytochrome c protein by employing mean fluorescence intensity measurements. The scopoletin-based MIP resulted in K_d values of 2.51×10^{-6} M and 8.5×10^{-6} M for the peptide and whole protein, respectively. A photochemically polymerized epitope MIP, synthesized for cytochrome c using a different monomer mixture, led to higher affinity (7.23×10^{-9} M), where a fluorescence-based NanoOrange protein assay was employed for target detection (Nishino et al., 2006). The electrochemical sensor developed in the current study using the CME imprints resulted in much higher sensitivity and affinity.

The detection of protein biomarkers were reported in the literature using different molecular imprinting techniques (Wang et al., 2018; Viswanathan et al., 2012; Ribeiro et al., 2018; Lu et al., 2012). For example, the detection limits of 2 ng mL^{-1}, 7.7 μg mL^{-1}, 0.5 U mL^{-1}, 0.10 U mL^{-1} were reported for HIV-1 glycoprotein (gp41), transferrin, CA 125 and CA15-3, respectively. The MIP for gp41 was prepared based on epitope imprinting using dopamine as a functional monomer (Lu et al., 2012). On the other hand, transferrin was imprinted using scopoletin by following whole protein imprinting approach (Zhang et al., 2018), resulting a much higher detection limit than that of the current work. Phenol (Viswanathan et al., 2012) and toluidine blue (Ribeiro et al., 2018) were used as the functional monomers for the preparations of CA 125 and CA15-3 MIPs by employing the electropolymerization technique.

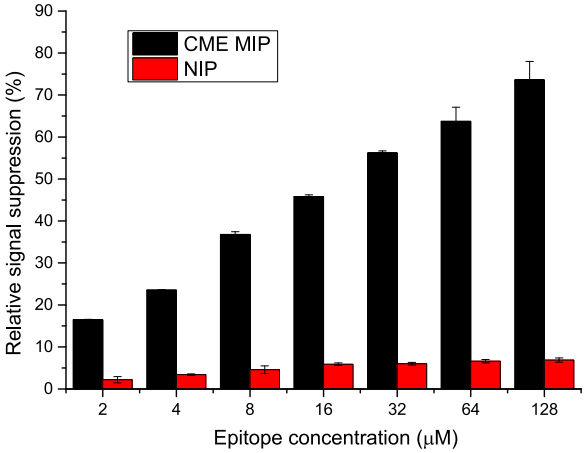

Fig. 2. Comparison of affinity binding between the cysteine-modified epitope MIPs (black columns) and the NIPs (red columns) for the NSE peptide detection. Imprinting factor (IF) = 8.8. (For interpretation of the references to colour in this figure legend, the reader is referred to the web version of this article.).

We further studied the selectivity of the imprinted cavities by investigating the binding of the NSE derived peptide on the MIP and NIP surfaces. Due to the absence of the cavities on the control polymer, the binding interaction of the target molecule with the NIP produced very low sensor signals (Fig. 2), suggesting weak interaction of the peptide with the control polymer. The imprinting factor was determined as 8.8 based on the comparative MIP and NIP assays, indicating a good selectivity of the CME imprints toward the target peptide.

3.3. Histidine-modified epitope imprinting

The formation of electro-synthesized HME imprints was followed by voltammetry techniques (Fig. 3). The CV curve of c in Fig. 3A illustrates the successful MIP preparation with the histidine-modified peptide entrapped in the polymer network. As a result this caused a significant signal suppression when compared to the bare gold wire (CV curve a). The optimum number of electro-polymerization cycles for this method was 30 using a multistep amperometry technique. The application of higher numbers of polymerization cycles led to insufficient template removal, which pointed to potentially buried templates remaining in the polymer network despite the application of a 40 min alkaline treatment. For template removal shorter (20 min) and longer (60 min) incubation times in alkaline solution (NaOH) were also examined, but these conditions resulted in poor rebinding capacities or led to almost complete removal of the MIP film from the gold surface. The optimal incubation time for template removal was determined as 40 min and this was confirmed by CV and SWV results. The peak heights of SWV at around 0.2 V were found to be 393 μA, 9 μA and 350 μA for the bare gold, the polymerization, and the template removal, respectively (Fig. 3B). Of note, the large current window between the polymerization and the template removal plays a key role for determination of the target molecules in a wide investigation range.

3.4. Target detection using histidine-modified epitope imprinting

The detection of the NSE derived peptide was achieved in a concentration range from 15.6 nM to 128 μM. The square wave voltammograms of the concentration-dependent peptide binding assays in the range of 15.6–1000 nM were demonstrated in Fig. 3C, where the increased concentration of the peptide sample led to a gradual decrease of the signal due to the lower level of electron transfer on a denser electrode surface. The overall results of six separate experiment series are given in Fig. 3D along with the Scatchard plot for affinity determination. The limit of detection (LOD) and K_d of the peptide assays were

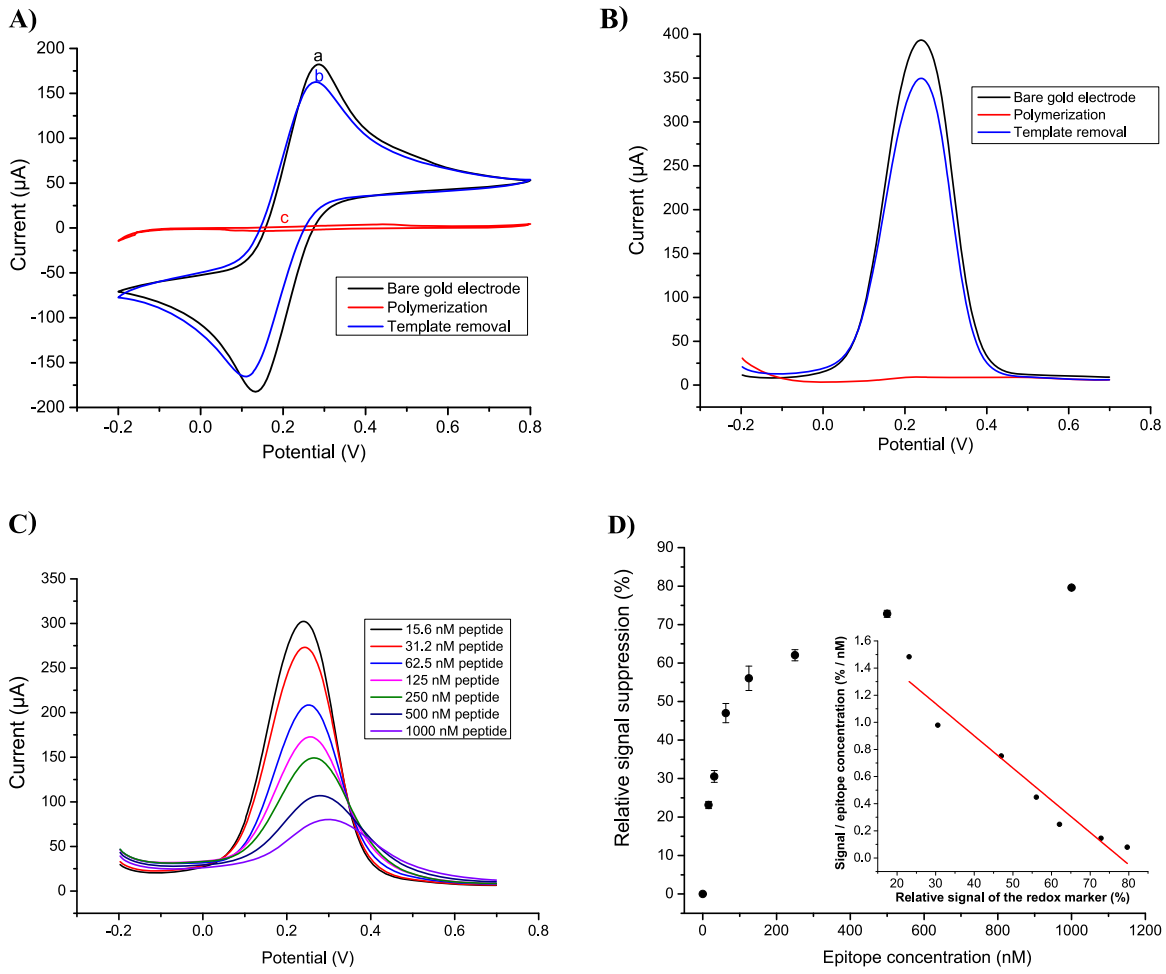

Fig. 3. A) Characterization of each step of the histidine-modified epitope MIP synthesis using CV: Voltammograms recorded in $K_3[Fe(CN)_6]$ (5 mM), $K_4[Fe(CN)_6]$ (5 mM)/potassium chloride (0.1 M) for bare gold electrode (a), template removal (b) and polymerization of scopoletin and the template (c). **B)** Following up the imprinting process using the SWV technique with the same redox marker solution. **C)** Square wave voltammetry detection of the NSE derived peptide with the histidine modified MIP cavities in the range of 15.6 − 1000 nM. **D)** Concentration dependent peptide detection using the MIP sensor. Inset: The Scatchard plot, $K_d = 4.2 \times 10^{-8}$ M.

found to be 15.6 nM and 4.2×10^{-8} M, respectively. Hence, compared to method 1 (CME-MIP, $K_d = 7.6 \times 10^{-6}$ M, LOD = 2 µM), the histidine-modified epitope imprinting approach (method 2) showed significantly higher affinity and sensitivity.

The comparative binding studies of the NSE derived peptide on NIP and MIP surfaces confirmed the high selectivity of the HME imprints toward the target molecule (Fig. 4A). The relative signal suppression of redox marker in the concentration range of 2–128 µM showed a regular gradual increase of the signal. The imprinting factor was evaluated by taking the sensor signal ratios between the MIP and the NIPs upon analyte binding on both surfaces. The imprinting factor of 11 was obtained, suggesting a high selectivity of the developed MIPs. Additionally, it can be stated that the NIPs, prepared in the absence of the template peptide, showed extremely low affinity toward the target peptide. This was also confirmed in the concentration range of 15.6–1000 nM with an IF of 12 (Fig. S8). The IF obtained with method 2 is therefore higher than method 1, which is in agreement with sensitivity and affinity data as well. Higher or lower IFs were reported in literature for scopoletin-based MIPs for other targets. For example, Dechtrirat et al. (2012) reported IFs of 10 and 6 for MIPs toward cytochrome c derived peptide and cytochrome c protein, respectively. Bosserdt et al. (2015) reported an imprinting factor of 13 for electro-synthesized ferritin MIP based on SPR technique. On the other hand, an IF of 5 was obtained for electro-synthesized transferrin MIP (Zhang et al., 2018).

As the next step, the recognition of NSE protein was investigated using the HME imprints, where the protein could be measured in the linear range of 0.25–64 ng mL^{-1} using the SWV technique (Fig. 4B). Compared to method 1 (LOD = 1 ng mL^{-1}), a four times higher sensitivity was achieved. As a result, the affinity of MIPs obtained with method 2 was higher toward the NSE biomarker (3×10^{-11} M, calculated based on the Scatchard plot in Fig. 4C). The clear differences in performances of the two different methods are most likely due to the more efficient template removal and the application of the histidine-modification in method 2. Moreover, some of CMEs may lie down on the surface and fold, therefore, their cavities can be less efficient and stable than those of HME imprints. We expect additional histidine in the peptide sequence resulted in more rigid structure and it possibly resided on the surface like a hook (in contrast with vertically adsorbed CMEs). Therefore peptide or protein could reach the cavities easier and bind stronger during the rebinding process. More importantly, we thought that electron density of imidazole ring in histidine influences the polymerization as it is charged. Ionic strength of buffer must be another factor for achieving better output with HME imprints. However, the other amino acid modifications should be investigated in epitope imprinting to have a better insight in this phenomenon. Such studies may also provide concrete information regarding the higher affinity of MIPs toward NSE when compared to NSE derived peptide.

Of note, the CME- and HME MIP sensors could be reused for eight and nine subsequent varied concentrations of target molecules, respectively.

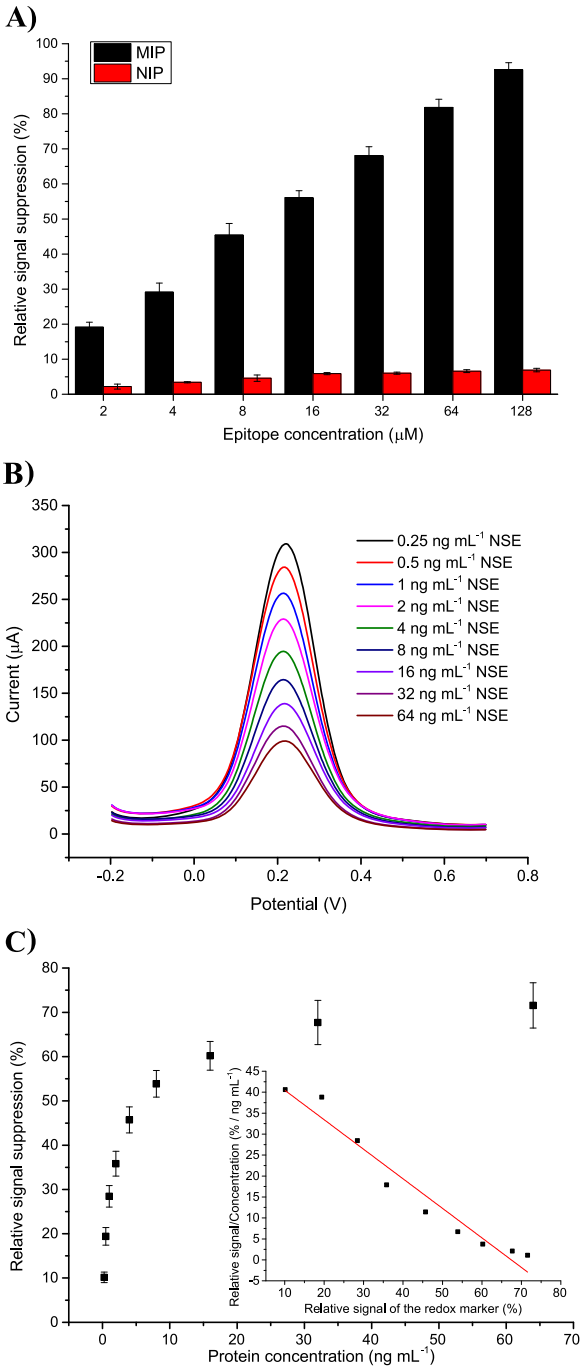

Fig. 4. A) Comparison of affinity binding between the histidine-modified epitope MIPs (black columns) and the NIPs (red columns) to determine the selectivity of the synthesized MIPs for the NSE derived peptide. Imprinting factor (IF) = 11. **B)** Square wave voltammograms showing the NSE biomarker detection in the concentration range of 0.25–64 ng mL^{-1} (signal suppression is proportional to the concentration of NSE loaded onto the MIP surface). **C)** Overall results of NSE binding assays using the histidine-modified epitope MIP sensor. Inset: Scatchard plot, $K_d = 3 \times 10^{-11}$ M. (For interpretation of the references to colour in this figure legend, the reader is referred to the web version of this article.).

Afterwards, the polymer surfaces reached the saturation level as all cavities were filled with target molecules. We also tried to regenerate the MIP electrodes using acidic (HCl) and basic (NaOH) solutions. However, these harsh conditions effected the polyscopoletin MIP layers. Wang et al. (2018) reported a MIP sensor for NSE detection by using whole protein imprinting approach. Their sensor could be successively used up to six times. However, protein imprinting is highly costly and the preparation of this sensor requires a long time. A detailed comparison of our HME MIP sensor and their sensor is provided in Table S1.

3.5. Cross reactivity assays

Using two different methods for the generation of MIPs we investigated the different specificities. Hence, the specific (NSE derived peptide and NSE protein) and non-specific (control peptide 1, control peptide 2 and BSA protein) analytes were prepared at a fixed concentration of 30 ng mL^{-1} and then incubated with the MIP electrodes for 30 min. The results were expressed as relative signal suppression data, where the binding of the NSE derived peptide to the histidine- and cysteine-modified epitope MIPs led to ~27% and 26% relative signal intensities, respectively. The non-specific binding of control peptide 1 resulted in ~3.5% and ~9.9% relative signal intensities, whereas they were ~5.6% and ~12.9% for control peptide 2, respectively. The specific binding of NSE protein to the histidine- and cysteine-modified epitope imprints produced ~68% and 45% relative signals, respectively. On the other hand, the cross-reactivity of BSA protein with the imprints resulted in ~7.5% and 15% relative signal intensities, respectively. It is worth mentioning that control peptide 2 possesses an α-helical structure with a cysteine modification on both ends. We used this sequence as a control peptide to check for possible interactions of the thiol side chain with the gold surface. However, it is clear that both MIPs liberated from the template formed stable and continuous films on the gold surface. Hence, the control peptide 2 could not interact with the gold surface (Fig. S9). Despite the control peptide 1 is also a surface exposed NSE epitope with a length of 10 amino acids, its non-specific binding on the MIP surfaces are at low levels, indicating the epitope specificity of the synthesized MIP via non-covalent interactions. To summarize, the specificity of histidine-modified epitope imprints was found to be clearly higher than that of cysteine-modified epitope imprints. More importantly, the two methods demonstrated significant differences for specific (NSE) and non-specific protein (BSA) binding on the MIP surfaces, where NSE produced a 33% higher signal and BSA resulted in 50% less cross-reactivity at a concentration of 30 ng mL^{-1} using HME imprints (Fig. S9).

3.6. AFM characterization of MIPs

The AFM measurements enable a deeper characterization of the synthesized MIPs on the gold electrode surface. The 2D and 3D surface topography images (Fig. 5, left and middle) along with cross-section profiles (Fig. 5, right) were recorded and analyzed for all stages of MIP and NIP preparation, i.e.: 1) the bare gold surface, 2) the densely covered surface of an imprinted polymer, 3) the MIP film after template removal and 4) the NIP film. The cleaned QCM surface acted as a reference point with an RMS value of 0.33 ± 0.01 nm and a maximum cross-sectional height of 1.45 nm (Fig. 5A, left and middle). The AFM images associated with electropolymerization of the monomer on pre-adsorbed peptide on the gold chip gave an RMS roughness of 10 ± 0.8 nm with a cross sectional height value of 51.7 nm (Fig. 5B). This is a significant increase compared to the bare QCM gold chip and confirms the formation of a thin polymer film in the nm range on the gold electrode. Removal of the peptide from the MIP cavities led to a further increase in the RMS roughness (11 ± 0.7 nm) and cross-sectional height (54 nm) as shown in Fig. 5C. After template removal the white rounded spots disappeared to a significant extent which led to a rougher surface with larger cross-sectional height. The AFM images of histidine-modified epitope MIPs demonstrated a similar trend with RMS values of 6.7 ± 0.7 nm and 9.0 ± 0.6 nm for the electropolymerized polymer film and the template-removed MIP, respectively (Fig. 5D and E). On the other hand, the AFM results for NIP showed clearly different results when compared to the MIP (Fig. 5E). As expected, the cross-section analysis and the topology images show an overall smoother

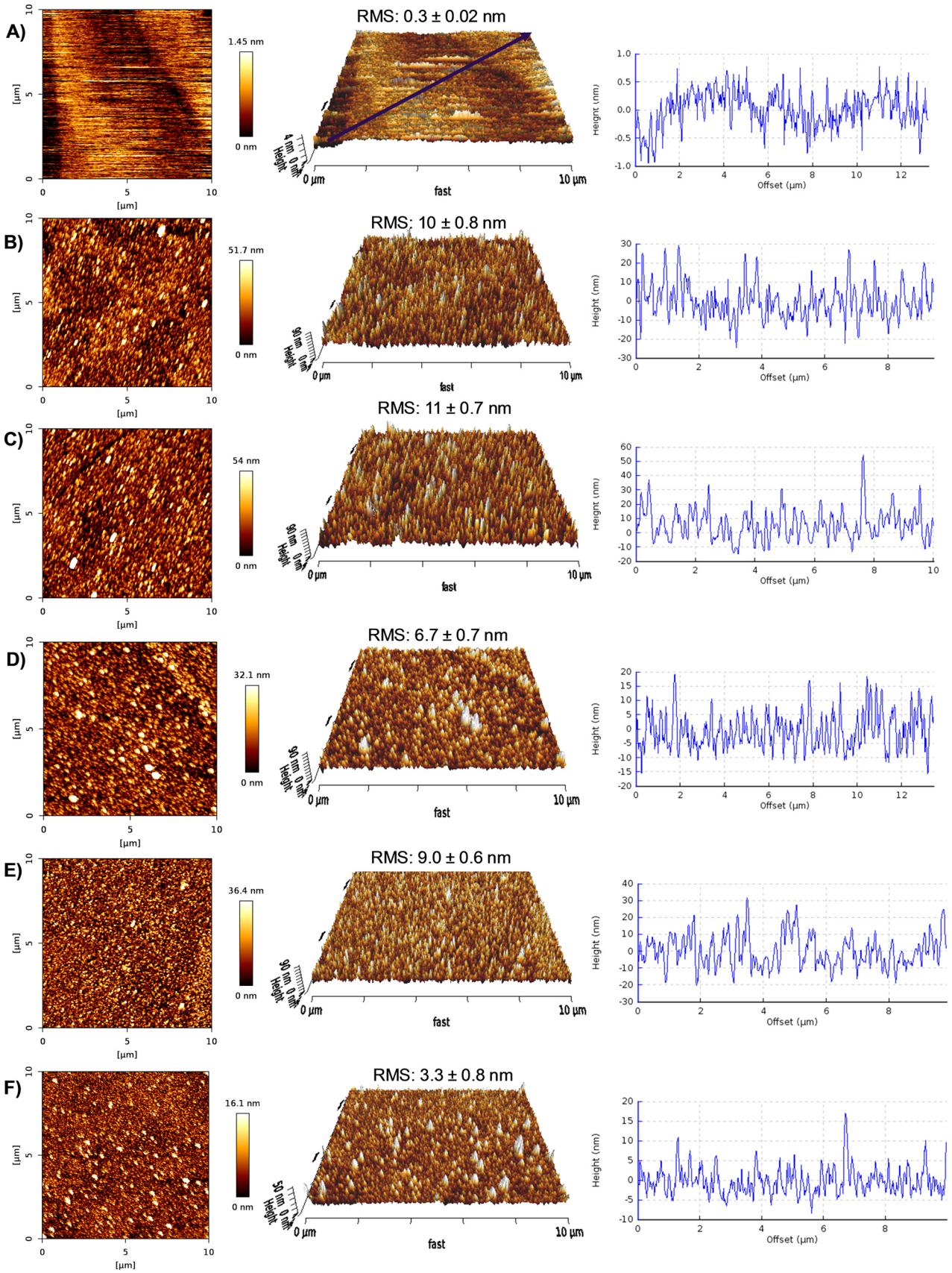

Fig. 5. AFM characterization of the bare gold chip (**A**), the templated cysteine-modified epitope MIP (**B**), the template free cysteine-modified epitope MIP (**C**), the templated histidine-modified epitope MIP (**D**), the template free histidine-modified epitope MIP (**E**) and NIP (**F**) in terms of 2D height images (left), 3D topography images (middle) and cross-section profiles (right). RMS values represent average results of 15 cross-sections along with the standard deviations.

surface for the NIP (3.3 ± 0.8 nm), varying in large parts at around 10 nm. Excluding the bare chip, which naturally has the smallest roughness (0.33 nm), a comparison of the RMS roughness of the samples (cysteine- and histidine-modified peptide MIP) results in two observations: Firstly, the roughness increased when changing from the templated surface to the template-removed MIP. This was expected, considering that the previously occupied cavities now become exposed to the surface. Secondly, the NIP film showed clearly lower roughness, indicating that no peptide was caught inside the polymer, resulting in an overall more homogeneous surface. These findings are in good agreement with the previously reported works on the AFM characterization of drug-imprinted polymers using the electropolymerization method (Pernites et al., 2011; Waffo et al., 2018). A summary and comparison of RMS values for every step of imprinting is provided in the Supplementary information (Table S2). To visualize the details of the MIP and NIP surfaces on the gold chip, we performed further AFM measurements in smaller scanning areas (i.e. 3 μm × 3 μm and 1 μm × 1 μm). The RMS values and cross-sectional profiles of the MIP and NIP surfaces provided similar outcomes (Figs. S10–S19) as obtained for the 10 μm × 10 μm scanning area. We also considered identifying the template-free MIPs by chemical mapping of the surfaces based on phase image analysis by AFM. The phase image is mainly characterized by different chemical components (Ye and Zhao, 2010). For example, there are continuous microdomains (colored light brown, Fig. S20A and B) on the templated MIP surfaces, revealing 26.2 and 27.1 degree phase lags for the histidine- and cysteine-modified epitope MIPs. Furthermore, there are significant changes on both surfaces after template removal (Fig. S20C and D), which led to two different morphological phases. The changes on the surfaces resulted in a higher degree phase lag for both MIPs. However, the difference was much higher for the histidine-modified epitope imprints (132 degree phase lag) than that of cysteine-modified epitope imprints (30.5 degree phase lag). Therefore, the two different phases (polymer film and cavities) on the surface were defined after template removal. However, the discrimination of the two phases was more satisfactory for the histidine-modified epitope MIPs than the cysteine-modified ones. This is most likely due to the more efficient template removal and thinner MIP film in the former case as a result of lower number of cycles for electropolymerization.

4. Conclusions

In this study, we developed novel biomimetic electrochemical sensors for rapid, sensitive and specific recognition of the small cell lung cancer biomarker NSE using cost-effective epitope imprinting approaches. The scopoletin-based MIPs targeting NSE derived peptide epitope as well as whole biomarker were synthesized via surface imprinting in the presence of cysteine- or histidine-modified epitope templates. The imprinted cavities created by cysteine- and histidine-modified epitopes could detect the peptide in a concentration range of 2–128 μM and 15.6 nM to 128 μM, respectively. The same template cavities allowed for the recognition of NSE in a linear range of 1–64 ng mL^{-1} and 0.25–64 ng mL^{-1}, respectively. The binding of the target molecules to the non-specific polymers was very little and the imprinting factors of 8.8 and 11 were determined for the CME and HME imprints at the same investigation range, respectively. The affinity analyses resulted in the dissociation constants of 2.31×10^{-10} M and 3×10^{-11} M for NSE recognition for corresponding epitope imprints, proving the higher affinity of histidine modified epitope imprinting toward the NSE biomarker. With regard to sensitivity, selectivity and specificity the histidine modification used for the surface imprinting turned out to be superior to the other method. The fabricated sensor using histidine modified epitope MIP demonstrate a great potential for protein recognition and detection. This promising strategy can be employed not only for NSE detection, but also for a wide range protein biomarkers.

Acknowledgement

This research was financially supported by European Commission and Maria Curie Actions under the project number 10041380. A partial funding was provided by the internal project of Technical University of Berlin (60320037-12).

Appendix A. Supporting information

Supplementary data associated with this article can be found in the online version at doi:10.1016/j.bios.2018.09.010.

References

Abdin, M.J., Altintas, Z., Tothill, I.E., 2015. Biosens. Bioelectron. 67, 177–183.
Altintas, Z., 2017. Biosensors and Nanotechnology: Applications in Health Care Diagnostics, first ed. John Wiley & Sons, New Jersey.
Altintas, Z., Tothill, I.E., 2013. Sens. Actuators B Chem. 188, 988–998.
Altintas, Z., Gittens, M., Guerreiro, A., Thompson, K.-A., Walker, J., Piletsky, S., Tothill, I.E., 2015a. Anal. Chem. 87 (13), 6801–6807.
Altintas, Z., Pocock, J., Thompson, K.-A., Tothill, I.E., 2015b. Biosens. Bioelectron. 74, 996–1004.
Altintas, Z., Guerreiro, A., Piletsky, S., Tothill, I.E., 2015c. Sens. Actuators B Chem. 213, 305–313.
American Cancer Society, 2017. Cancer Facts & Figures 2017. American Cancer Society.
Bosserdt, M., Erdőssy, J., Lautner, G., Witt, J., Köhler, K., Gajovic-Eichelmann, N., Yarman, A., Wittstock, G., Scheller, F.W., Gyurcsányi, R.E., 2015. Biosens. Bioelectron. 73, 123–129.
Cao, Z., Li, Huan, Lau, Choiwan, Zhang, Y.,, 2011. Anal. Chim. Acta 698, 44–50.
Cecchini, A., Raffa, V., Canfarotta, F., Signore, G., Piletsky, S., MacDonald, M.P., Cuschieri, A., 2017. Nano Lett. 17 (4), 2307–2312.
Chen, H.-J., Zhang, Z.-H., Luo, L.-J., Yao, S.-Z., 2012. Sens. Actuators B Chem. 163, 76–83.
Chen, L., Wang, X., Lu, W., Wu, X., Li, J., 2016. Chem. Soc. Rev. 45, 2137–2211.
Cieplak, M., Szwabinska, K., Sosnowska, M., Chandra, B.K.C., Borowicz, P., Noworyta, K., D'Souza, F., Kutner, W., 2015. Biosens. Bioelectron. 74, 960–966.
Cooper, E.H., 1994. Neuron-specific enolase. Int. J. Biol. Marker 9, 205–210.
Cooper, E.H., Splinter, T.A., Brown, D.A., Muers, M.F., Peake, M.D., Pearson, S.L., 1985. Br. J. Cancer 52, 333–338.
Dechtrirat, D., Jetzschmann, K.J., Stöcklein, W.F.M., Scheller, F.W., Gajovic-Eichelmann, N., 2012. Adv. Funct. Mater. 22, 5231–5237.
Erdossy, J., Horváth, V., Yarman, A., Scheller, F.W., Gyurcsányi, R.E., 2016. Trends Anal. Chem. 79, 179–190.
Feng, X., Gan, N., Zhou, J., Li, T., Cao, Y., Hu, F., Yu, H., Jiang, Q., 2014. Electrochim. Acta 139, 127–136.
Fu, X., Meng, M., Zhang, Y., Yin, Y., Zhang, X., Xi, R., 2012. Anal. Chim. Acta 722, 114–118.
Hoshino, Y., Koide, H., Urakami, T., Kanazawa, H., Kodama, T., Oku, N., Shea, K.J., 2010. J. Am. Chem. Soc. 132 (19), 6644–6645.
Huang, L., Zhou, J.-G., Yao, W.-X., Tian, X., Lv, S.-P., Zhang, T.-Y., Jin, S.-H., Bai, Y.-J., Ma, H., 2017. Oncotarget 8 (38), 64358–64372.
Jetzschmann, K.J., Yarman, A., Rustam, L., Kielb, P., Urlacher, V.B., Fischer, A., Weidinger, I.M., Wollenberger, U., Scheler, F.W., 2018. Colloids Surf. B Biointerfaces 164, 240–246.
Karimian, N., Turner, A.P.F., Tiwari, A., 2014. Biosens. Bioelectron. 59, 160–165.
Kryscio, D.R., Fleming, M.Q., Peppas, N.A., 2012. Macromol. Biosci. 12, 1137–1144.
Lautner, G., Kaev, J., Reut, J., Öpik, A., Rappich, J., Syritski, V., Gyurcsányi, R.E., 2011. Adv. Funct. Mater. 21, 591–597.
Li, H.-X., Xu, X.-L., Chen, H., Zhang, S., Kong, J.-L., 2012. Chin. J. Anal. Chem. 40, 817–822.
Lu, C.H., Zhang, Y., Tang, S.F., Fang, Z. Bin, Yang, H.H., Chen, X., Chen, G.N., 2012. Biosens. Bioelectron. 31, 439–444.
Marangos, P.J., 1987. Annu. Rev. Neurosci. 10, 289–295.
Moreira, F.T.C., Sharma, S., Dutra, R.A.F., Noronha, J.P.C., Cass, A.E.G., Sales, M.G.F., 2014. Sens. Actuators B Chem. 196, 123–132.
Nishino, H., Huang, C.-S., Shea, K.J., 2006. Angew. Chem. Int. Ed. 45 (13), 2392–2396.
Pernites, R., Ponnapati, R., Felipe, M.J., Advincula, R., 2011. Biosens. Bioelectron. 26, 2766–2771.
Ribeiro, J.A., Pereira, C.M., Silva, A.F., Sales, M.G.F., 2018. Biosens. Bioelectron. 109, 246–254.
Schmidt, F.M., Mergl, R., Stach, B., Jahn, I., Gertz, H.-J., Schonknecht, P., 2014. Neurosci. Lett. 570, 81–85.
Shibayama, T., Ueoka, H., Nishii, K., Kiura, K., Tabata, M., Miyatake, K., Kitajima, T., Harada, M., 2001. Lung Cancer 32 (1), 61–69.
Stojanovic, Z., Erdőssy, J., Keltai, K., Scheller, F.W., Gyurcsányi, R.E., 2017. Anal. Chim. Acta 977, 1–9.
Vermuyten, K., Lowenthal, A., Karcher, D., 1990. Clin. Chim. Acta 187 (2), 69–78.
Viswanathan, S., Rani, C., Ribeiro, S., Delerue-Matos, C., 2012. Biosens. Bioelectron. 33, 179–183.
Waffo, A.F.T., Yesildag, C., Caserta, G., Katz, S., Zebger, I., Lensen, M.C., Wollenberger, U., Scheller, F.W., Altintas, Z., 2018. Sens. Actuators B Chem. 275, 163–173.
Wang, X., Wang, Y., Ye, X., Wu, T., Deng, H., Wu, P., Li, C., 2018. Biosens. Bioelectron. 99, 34–39.
Wulff, G., Sarhan, A., 1972. Angew. Chem. Int. Ed. 11 (4), 341–344.
Ye, Z., Zhao, X., 2010. J. Microsc. 238, 27–35.
Zhang, X., Yarman, A., Erdossy, J., Katz, S., Zebger, I., Jetzschmann, K.J., Altintas, Z., Wollenberger, U., Gyurcsányi, R.E., Scheller, F.W., 2018. Biosens. Bioelectron. 105, 29–35.